Application of Sensory Body Schemas to Path Planning for Micro Air Vehicles (MAVs)

Eniko T. Enikov[1] and Juan-Antonio Escareno[2]
[1]*Department of Aerospace and Mechanical Engineering, University of Arizona, 1130 N. Mountain Ave, Tucson, AZ 85721, U.S.A.*
[2]*Directorate for Research and Innovation (DRII), Institut Polytechnique des Sciences Avancées (IPSA), 7-9 Rue Maurice Grandcoing, Ivry-sur-Seine, 94200, France*

Keywords: Micro-Air Vehicles, Artificial Neural Network, Path Planning, Body Schema, Cognitive Robotics.

Abstract: To date, most autonomous micro air vehicles (MAV-s) operate in a controlled environment, where the location of and attitude of the aircraft are measured be dedicated high-power computers with IR tracking capability. If MAV-s are to ever exit the lab and carry out autonomous missions, their flight control systems needs to utilize on-board sensors and high-efficiency attitude determination algorithms. To address this need, we investigate the feasibility of using body schemas to carry out path planning in the vision space of the MAV. Body schemas are a biologically-inspired approach, emulating the plasticity of the animal brains, allowing efficient representation of non-linear mapping between the body configuration space, i.e. its generalized coordinates and the resulting sensory outputs. This paper presents a numerical experiment of generating landing trajectories of a miniature rotor-craft using the notion of body and image schemas. More specifically, we demonstrate how a trajectory planning can be executed in the image space using a pseudo-potential functions and a gradient-based maximum seeking algorithm. It is demonstrated that a neural-gas type neural network, trained through Hebbian-type learning algorithm can learn a mapping between the rotor-craft position/attitude and the output of its vision sensors. Numerical simulations of the landing performance of a physical model is also presented, The resulting trajectory tracking errors are less than 8 %.

1 INTRODUCTION

The applications of Miniature Air Vehicles (MAVs) have widely diversified during the last five years. They comprise both military and civilian, though the latter has had a lower development rate. The main goal of unmanned air vehicles (UAVs) is to provide a remote and mobile extension of human perceptions, allowing not only the security of the user (soldier, policeman, cameraman, volcanologist), but also the collection of valuable information of zones/targets of interest used for on-line or off-line analysis. Rotorcraft MAVs represent an excellent alternative due to their versatile flight profile as hovering, vertical take-off/landing (VTOL) and maneuverability, allowing the access to small enclosures and navigation within unstructured environments. The enhanced proficiency of recently developed navigation and control algorithms has brought about the possibility of using VTOL MAVs in other civilian applications such as wildlife studies, urban surveillance (car and pedestrian traffic), and pollution monitoring, to mention just a few.

Despite the great number of potential MAV-based applications, the operational role of these air robots remains limited to being passive agents during their missions such as in surveillance tasks. Enhancing the current profile of MAVs implies endowing them with the ability to perform autonomous decision making, for example, an ability to establish a landing site, navigate to it, and land/perch. To date, almost all MAV research is carried out in a controlled laboratory environment where both the target landing location, as well as the MAV position are measured in real-time using a complex IR vision tracking system. If MAVs are ever to exit the lab, their flight control needs to be autonomous and based on on-board image and altitude sensors. To address this need, we proposed to utilize a biologically inspired approach emulating the plasticity of avian and human brain.

Traditionally, MAV controllers are derived from linearized models of the vehicle. The stability of these

Enikov E. and Escareno J..
Application of Sensory Body Schemas to Path Planning for Micro Air Vehicles (MAVs).
DOI: 10.5220/0005547000250031
In *Proceedings of the 12th International Conference on Informatics in Control, Automation and Robotics* (ICINCO-2015), pages 25-31
ISBN: 978-989-758-122-9

controllers is therefore limited to relatively small roll and pitch angles, while in the case of fast maneuvers, it is not guaranteed. Machine learning techniques have been successful in learning models based on data from human pilots (Abbeel et al., 2007), in improving performance of control using reinforcement learning (Lupashin et al., 2010), and exploring aggressive maneuvers such as fast translation and back flip (Purwin and D'Andrea, 2009; Gillula et al., 2011). In contrast to these prior efforts, the approach proposed here does not simply replicate the control of human operators, rather, it is based on the premise that through self-learning, the robot can create its own representation of its body and vision system and, upon a period of training, can learn to perform such maneuvers on its own. More specifically, we demonstrate the application of an artificial neural network representation of the robot's vision and attitude systems capable of controlling the robot to a target landing site. The property of ANN to provide control laws through implicit inversion of the robot's kinematic chain or in our case the non-linear transformation between vision system's output and the robot's attitude and position vectors is one of the main advantages of the proposed ANN-based approach. The specific type of ANN explored here is a self-organizing map (SOM) where artificial neurons participate in a competitive learning process, allowing the network to "discover" the body of the robot they describe. This process known as body schema, originally developed in the field of cognitive robotics, is a cornerstone of the proposed effort. The concept of a body schema was first conceived by Head and Holmes (Head and Holmes, 1911) who studied how human perceive their bodies. Their definition of body schema is a postural model of the body and its surface which is formed by combining information from proprioceptive, somatosensory and visual sensors. According to their theory, the brain uses this model to register the location of sensation on the body and control its movements. A classical example supporting the notion of body schema is the phantom limb syndrome, where amputees report sensations or pain from their amputated limb (Melzack, 1990; Ramachandran and Rogers-Ramachandran, 1996). Recent brain imaging studies have indeed confirmed that body schema is encoded in particular regions of the primate and human brains (Berlucchi and Aglioti, 1997; Graziano et al., 2000) along with body movements (Berthoz, 2000; Graziano et al., 2002). More importantly, it is now apparent that the body schema is not static, and can be modified dynamically to include or "extend" the body during use to tools (Iriki et al., 1996) or when wearing a prosthetic limb (Tsukamoto, 2000). These and other advances of cognitive neuroscience have led to the development of novel robot control schemes.

The pliability of body schemas is one of the main reasons a growing number of roboticists are exploring the use of various schemas, i.e. motor, tactile, visual in designing adaptable robots, capable of acquiring knowledge of themselves and their environment. Recent experiments in cognitive developmental robotics have demonstrated that using tactile and vision sensors, a robot could learn its body schema (image) through babbling in front of a camera viewing its arms, and subsequently, using a trained neuronal network representing its motion scheme, acquire an image of its invisible face through Hebbian self-learning (Fuke et al., 2007). Yet another study demonstrated an ability of a robot to extend its body schema to include a tool (a stick), without a need to re-learn its forward kinematics, rather, a simple shift in the sensory field (schema) of the robot was sufficient to reproduce the task of reaching a particular point in space with the stick (Stoytchev, 2003).

In this paper we extend the computational approach introduced by Morasso (Morasso and Sanguineti, 1995) which creates a link between the robot's configuration and sensor spaces utilizing a self-organizing map (SOM). In the case of an MAV, in addition to the vision system, the MAV sensor space includes vehicle's pitch angle. The trained network is then used to create a mapping between the configuration and sensor spaces, thus presenting a self-learned body schema. A unique feature of the approach is that the robot control task does not require the use of inverse kinematics, i.e. prediction of the robots' position and orientation in the global Cartesian space. Instead, through the use of a pseudo potential fields defined in the sensor space , the MAV is controlled to the desired landing position and orientation using an implicit inversion of the non-linear mapping between configuration and sensor spaces. These features of the proposed control scheme are illustrated in a 3-DOF planar MAV model described in the subsequent sections of this paper. In order to implement the proposed approach it is required the fusion of inertial and visual information, as demonstrated through simulations in this paper.

2 SELF-ORGANIZING BODY SCHEMA OF MAV-S

2.1 3-DOF MAV Model

The quadrotor is modeled as a 3D free-moving (trans-

lation and rotation) rigid body of mass m, concentrated at the center of gravity CG of the UAV. The motion of the flying robot can be expressed w.r.t. two coordinate systems: (i) the inertial frame $\mathcal{F}^i = (e_x, e_z)^T$, and ($ii$) the body frame $\mathcal{F}^b = (e_1, e_3)^T$, where e_u, e_w are the roll and yaw axes. An external translational force vector $\mathbf{T}$ is exerted on rigid-body's CG through the collective thrust of the rotors. Likewise, a torque $\tau^b = (0,T)^T$ is generated about CG by the differential thrust of the rotors. The equation modeling the 2D translational and rotational motion of the MAV are given by the well-known expressions (for details see (esc, 2007), (Goldstein, 1980) and (Fantoni and Lozano, 2002))

$$\left\{ \begin{array}{rcll} \dot{\xi}^i & = & \mathbf{V}^i & \\ (M+m)\dot{\mathbf{V}}^i & = & \mathbf{U}_\xi & \in \mathbb{R}^2 \\ I_Y \ddot{\theta} & = & U_\theta + \Gamma_m & \in \mathbb{R}^1 \end{array} \right. \quad (1)$$

where $\dot{\xi} = (\dot{x}, \dot{z})^T$ represents the 2D translational velocity of the drone, $\mathbf{U}_\xi = \mathcal{R}^\theta \mathbf{F}^b$ the projected thrust vector used as control of the translational subsystem, being $\mathbf{F}^b = (0,T)$, $\mathbf{W}_{(\mathbf{M+m})} = (0, -(M+m)g)^T$ is the total weight vector, while Γ_m corresponds to the torque introduced by the gear,

$$\Gamma_m = -mgl \sin\theta \quad (2)$$

The MAV's configuration coordinates are the lateral and vertical positions of its center of mass, x, and z, respectively, and its pitch angle, θ, (see Fig. 1). The output of the vision system can be any feature in

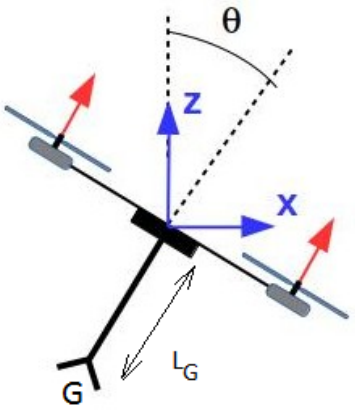

Figure 1: 3DOF model of a planar rotor craft.

the image space, and in particular, the location of the robot's landing gear, G (represented as inverted Y in Figure 1. For illustrative purposes and without loss of generality, we consider an idealized vision system where the coordinates of the MAV's landing gear in the camera's image plane (x_C, y_C) are replaced with the actual coordinates of the landing gear (x_G, z_G) in the Cartesian space of motion of the MAV. Additionally, the pitch angle θ is measured by an on-board inertial measurement unit (IMU). The triplet (x_G, y_G, θ) thus represents a fusion of vision and IMU sensor data.

A non-linear transformation exists between the generalized position of the center of mass determined by the triplet (x, z, θ) and the location of the landing gear

$$\left\{ \begin{array}{c} x_G \\ z_G \\ \theta \end{array} \right\} = \left\{ \begin{array}{c} x - L_G \sin\theta \\ z - L_G \cos\theta \\ \theta \end{array} \right\} \quad (3)$$

In what follows, we will demonstrate how an MAV can learn transformation (3) using a self-organizing body schema and apply the learned transformation to navigate to a landing target.

2.2 Body and Sensor Schemas

The self-organizing body schema (So-BoS) links the robot's sensor space $\mathcal{S}$ with is configuration space $\mathcal{C}$. It utilizes a single $\mathcal{CS}$-space=$\mathcal{C} \times \mathcal{S}$ to identify the robot configuration as well as to plan motion in the robot's sensor space. A detailed review of applications of body schema-s in robotics can be found in (Hoffmann et al., 2010). As an extension of the approach of Morasso (Morasso and Sanguineti, 1995) and Stoychev (Stoytchev, 2003), in addition to vision data, the sensor space includes vehicle attitude (pitch angle θ), measured by an on-board artificial horizon sensor or attitude gyro. Similar to conventional self-organizing neural network maps, a layer of neurons (processing units) is used to learn the mapping between the configuration space (generalized position of the robot) and the output of the vision system (the location of its landing gear). Unlike other topologically ordered self-organizing maps such as the Kohonnen map (Kohonen, 1982), the neurons in the present approach are initially disordered, i.e. forming a ''neural gas" (Martinetz et al., 1991). The training process modifies the weights of each neuron until the network learns N body icons representing the $\mathcal{CS}$-space. More specifically, denoting by $\mu = [x, z, \theta]$ the robot's generalized position coordinates, and by $\beta = [x_G, z_G, \theta]$ the vector of vision and attitude sensor outputs, then for each body position i, the generalized coordinates and associated sensors outputs will present an instance of these two vectors $\tilde{\mu}_i = [\tilde{x}^i, \tilde{z}^i, \tilde{\theta}^i] \in \mathcal{C}$ and $\tilde{\beta}_i = [\tilde{x}^i_G, \tilde{z}^i_G, \tilde{\theta}^i] \in \mathcal{S}$, respectively. The matched pairs $(\tilde{\beta}_i, \tilde{\mu}_i) \in \mathcal{CS}$ are referred to as body icons. The $\mathcal{CS}$ space is approximately by a field of N neurons, each storing a learned body icon $(\tilde{\beta}_i, \tilde{\mu}_i), i = 1, \ldots N$. Associated with each neuron is an activation function, $U_i(\mu)$, which in this case is chosen to be the softmax

function given by

$$U_i(\mu) = \frac{G\|\mu - \tilde{\mu}_i\|}{\sum_j G(\|\mu - \tilde{\mu}_i\|)},$$

where G is a Gaussian function with variance σ^2. The normalization of $U_i(\mu)$ ensures that it has a maximum at $\mu = \hat{\mu}_i$. The choice of σ determines the range of activation of neighboring neurons when computing the response of the network through

$$\mu^{approx} = \sum_j^N \tilde{\mu}_j U_j(\mu). \quad (4)$$

Similarly, the output of the sensory system is produced by

$$\beta^{approx}(\mu) = \sum_j^N \tilde{\beta}_j U_j(\mu). \quad (5)$$

The network training process is based on a competitive learning process, where the N neurons are presented with a large number of pseudo-random training vectors $\hat{\mu}_l, l = 1, \ldots I$. In the present example $N = 300$ and $I = 950$. For each training cycle, all training vectors $\hat{\mu}_l$ are presented to the network and the body icons are updated according to their respective learning laws

$$\Delta\tilde{\mu}_j = \eta_1(\hat{\mu}_l - \tilde{\mu}_j)U_j(\hat{\mu}_l) \quad (6)$$

and

$$\Delta\tilde{\beta}_j(\mu) = \eta_2(\beta - \tilde{\beta}_j)U_j(\hat{\mu}_l). \quad (7)$$

The parameters η_1 and η_2 are the learning rates for each law, respectively. The competitive learning process involves reduction of the learning rate as well as the range of activation specified by σ as the training proceeds. Through (5, the trained network represents a mapping between the MAV-s generalized position (C configuration space) and the resulting sensor space $\mathcal{S}$. Therefore, it is an implicit calibration procedure. Figure 2 presents the 950 training vectors (blue dots) and the learned body icons (green circles) upon training of $N = 300$ through $N_T = 50$ training cycles. The starting learning rates are $\eta - 1 = \eta_2 = 3.84$, with variance $\sigma^2 = 10/3$. All three parameters were reduced linearly to $1/N_T$ of their starting values at the end of the last training epoch.

One of the greatest benefits from the trained neural network and the associated mapping (5) is its ability to generate robot trajectories in the sensor space without explicitly computing its inverse Jacobian. This property of the body-schema based approach is illustrated in the next section.

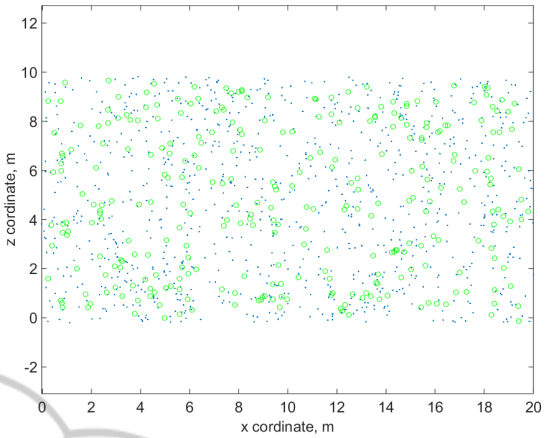

Figure 2: Training Set (blue dots) and Resulting Learned Body Icons (green circles). Each green marker represents a set of (x_G, y_G, θ) body icon (position) learned by its corresponding neuron.

3 TRAJECTORY PLANNING IN THE IMAGE SPACE

Upon training, each processing unit has its preferred body icon $(\tilde{\beta}_i, \tilde{\mu}_i)$ allowing representation of the MAV's sensory output through (5). In addition to the sensory output, the trained network can define additional functions over the MAV's configuration space or the sensory space. One particularly interesting application is path planning in the sensor space which is useful for landing or navigation. The advantage of the method is that the trained network does not require explicit inversion of the mapping between the robot's position and the output of the vision and navigation sensors. Instead, the trajectory can be obtained through solution of a ordinary differential equation providing the position and velocity of the MAV. More specifically, we use a pseudo-potential defined over the vision space of the MAV defined through

$$\xi(\mu) = \sum_j \tilde{\xi}_j(\hat{\beta})U_j(\mu), \quad (8)$$

where $\tilde{\xi}_j$ are scalar weights for each processing unit. The potential weights can be selected such, that the resulting pseudo-potential has an extrema (for example maximum) at the target landing location. Then a simple ordinary differential equation can be formulated that has a maximum- or minimum-seeking solution. Following the method of (Stoytchev, 2003), we use a gradient ascend equation to drive the MAV's generalized coordinates to the maximum of the pseudo-potential

$$\dot{\mu} = \gamma\nabla\xi(\mu) = \gamma\sum_{j=1}^N (\tilde{\mu}_j - \mu)\xi_j U_j(\mu). \quad (9)$$

The desired landing location, including the landing angle, can be specified by the choice of $\xi_j(\hat{\beta})$. The right-hand side of (9) provides the velocities of the MAV, while its solution generates the landing trajectory.

To illustrate the approach, we have used two possible landing sites marked T1 and T2 in Figure 4.The landing site T1 is at $x_a = 6, z_a = 2, \theta_a = 0°$, while the T2 is at $x_a = 19, z - a = 5, \theta_a = 30°$. The corresponding pseudo-potential is defined as

$$\xi_a(\mu) = \frac{1}{\|\beta_a - \beta(\mu)\|}, \qquad (10)$$

where $\beta_a = (x_a, z_a, \theta_a)$. The actual weights are computed by evaluating (10) for each processing unit j, i.e. $\tilde{\xi}_j = \xi_a(\tilde{\mu}_j)$. The corresponding pseudo-potential

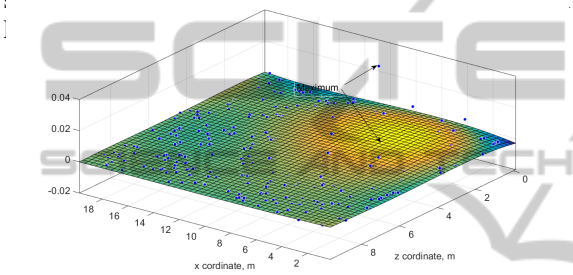

(a)

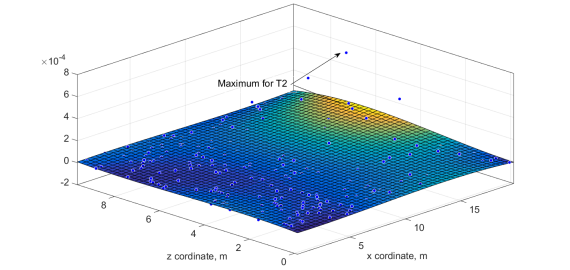

(b)

Figure 3: Pseudopotential surface *xi* for target location T1 (a) and T2 (b). The surface is represented by a 4-th order polynomial fit over the actual values of the potential function xi_i marked with blue dots.

Solving equation (9) for each of the target landing sites T1 and T2 results in 24 trajectories emanating from S1-S12 for eatch of the two targets as shown in Fig. 4.

4 EVALUATION OF TRAJECTORY TRACKING

The data generated from the path-planning step described in the previous section was fed into a calibrated model of a rotor-craft (Escareno et al., 2013). The physical parameters of the MAV rotorcraft were $m = 0.4$ kg, $I_{yy} = 0.177$ kg-m^2, operating in Earth's gravitational field $g = 9.81$ m/s^2. Four resulting actual trajectories leading to the desired target T1 were generated as shown in Figure 5. As can be observed there is a transient error of approximately 1.5 m at the beginning of some trajectories, along with a small overshoot needed to absorb the kinetic energy of the rotor-craft. A complementary test was carried out to observe the behavior of the proposed approach with respect to a classical regulation problem. Figures 7 depict the performance of the NN-based tracking and the regulation controllers to reach the landing coordinates. In such figure it is observed that angular behavior is smooth compared with classical angular regulation.

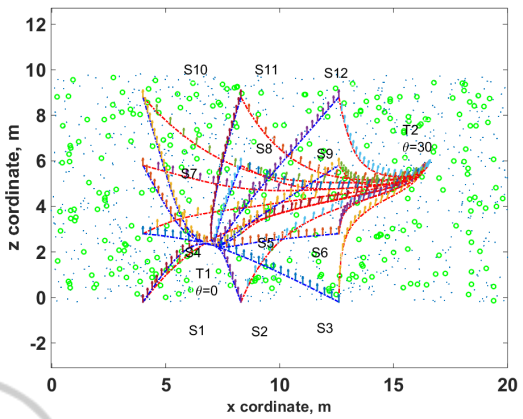

Figure 4: Simulated robot paths to two different target locations (T1 and T2) in the robot's vision space.The arrows in the figure represent the MAV pitch angle.

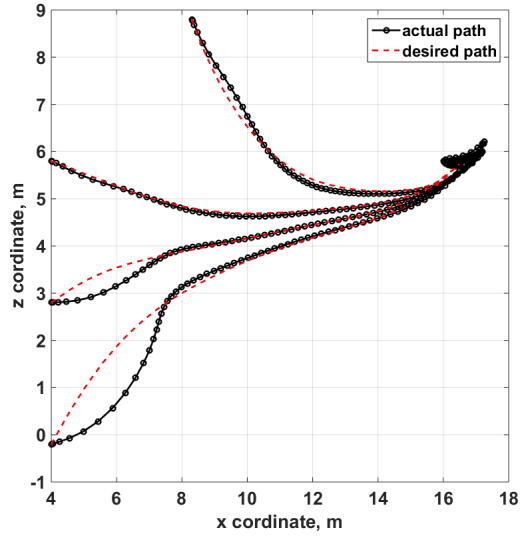

Figure 5: MAV trajectory tracking performance using the ANN-generated landing trajectories to T2.

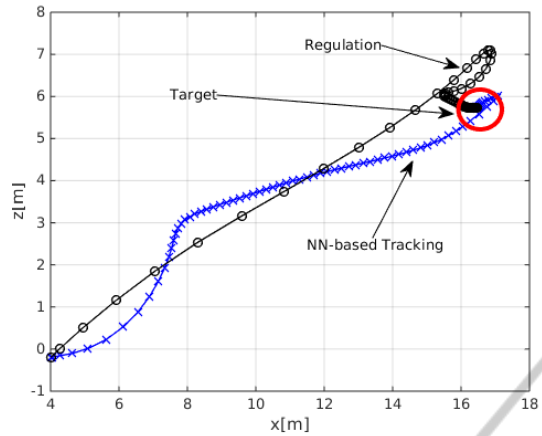

Figure 6: Comparative between the NN-based tracking and a classical regulation control.

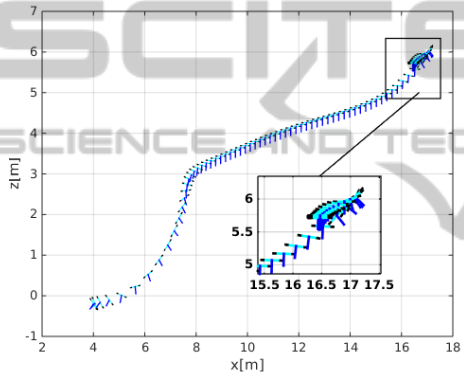

(a)

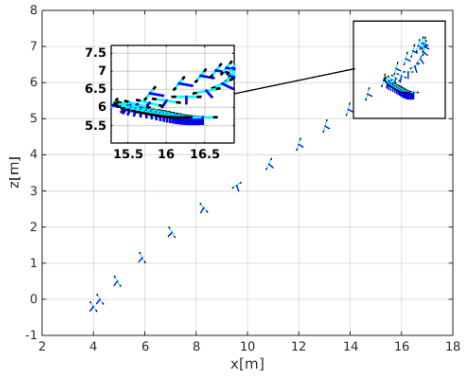

(b)

Figure 7: Behavior of the rotorcraft: [a] NN-bases tracking control [b] Classical regulation.

4.1 Two-Time Scale Controller

It has been used a classical two-time scale controller to fulfill the tracking objective for the translational dynamic subsystem (1a), where it is defined a linear behavior through stable error polynomials $u_x(e_x, \dot{e}_x)$ and $u_z(e_z, \dot{e}_z)$ as presented in (Sepulchre et al., 1997).

$$\begin{aligned} \ddot{x} &= T\sin\theta &:=\ & u_x(e_x, \dot{e}_x) \\ \ddot{z} &= T\cos\theta - g &:=\ & u_z(e_z, \dot{e}_z) \end{aligned} \tag{11}$$

with $u_x = k_{p_x} e_x + k_{v_z} \dot{e}_x$ and $u_z = k_{p_z} e_z + k_{v_z} \dot{e}_z$. Such stable linear behavior is achieved if

$$T = \left[u_x^2 + (u_z + g)\right]^{\frac{1}{2}} \tag{12}$$

$$\theta = \theta_d(t) \text{ with } \theta_d(t) = \arctan\left(\frac{r_1}{r_2 + g}\right) \tag{13}$$

with k_{p_q}, k_{p_z} and k_{v_z} are positive constants. The latter assumes a time-scale separation between translation (slow dynamics) and rotational (fast dynamics) motion. The latter assumes a time-scale separation between translation (slow dynamics) and rotational (fast dynamics) motion. Thus, from the error variable $\tilde{\theta} = \theta - \theta^d$ arises the following dynamics

$$\ddot{\tilde{\theta}} = \tau_\theta - \ddot{\theta}^d \tag{14}$$

where $\ddot{\theta}^d$ is disregarded to avoid aggressive commands. The controller aims to track $\theta^d(t)$ while compensating the torque induced by the gear, for this purpose it is used the controller

$$u_\theta = -k_{p_\theta} e_\theta - k_{v_\theta} \dot{e}_\theta + mgl\sin\theta \tag{15}$$

5 SUMMARY AND CONCLUSIONS

The application of self-organizing artificial neural networks to the problem of path planning of MAV-s have been described. It has been demonstrated that the neural network can fuse seamlessly the information gathered from different sensory outputs such as vision and attitude sensors. Upon training period comprised of carrying out pseudo-random motions, akin birds learning how to fly, the MAV can learn landing maneuvers leading to the desired landing position. The accuracy of the landing has been found to depend on the number of nodes used in the artificial neural network as well as the training parameters such as learning rate and range of activation of the neuronal network. The resulting trajectories of the physical model show transient errors of approximately 8 % (1 .5 m over a landing target at 18 m) and a small overshoot of 0.7 m (4. %) required to reduce the landing speed. Due to its low computational demand upon completion of the ANN training, the proposed method is likely to find application in the development of bio-inspired MAV-s capable of autonomous navigation using low-cost vision and attitude sensors.

ACKNOWLEDGEMENTS

The authors acknowledge the support of IPSA in hosting one of the authors (Enikov) during his sabbatical leave allowing the development of this collaborative research project as well as partial support from NSF grant # 1311851 related to the development of ANN simulation library.

REFERENCES

(2007). *Embedded control system for a four rotor UAV*, volume 21.

Abbeel, P., Coates, A., Quigley, M., and Ng, A. Y. (2007). An application of reinforcement learning to aerobatic helicopter flight. *Advances in neural information processing systems*, 19:1.

Berlucchi, G. and Aglioti, S. (1997). The body in the brain: neural bases of corporeal awareness. *Trends in neurosciences*, 20(12):560–564.

Berthoz, A. (2000). *The brain's sense of movement*. Harvard University Press.

Escareno, J., Rakotondrabe, M., Flores, G., and Lozano, R. (2013). Rotorcraft mav having an onboard manipulator: Longitudinal modeling and robust control. In *Control Conference (ECC), 2013 European*, pages 3258–3263. IEEE.

Fantoni, I. and Lozano, R. (2002). *Nonlinear control for underactuated mechanical systems*. Springer.

Fuke, S., Ogino, M., and Asada, M. (2007). Body image constructed from motor and tactile images with visual information. *International Journal of Humanoid Robotics*, 4(02):347–364.

Gillula, J. H., Huang, H., Vitus, M. P., and Tomlin, C. J. (2011). Design and analysis of hybrid systems, with applications to robotic aerial vehicles. In *Robotics Research*, pages 139–149. Springer.

Goldstein, H. (1980). *Classical mechanics*. Addison-Wesley.

Graziano, M. S., Cooke, D. F., and Taylor, C. S. (2000). Coding the location of the arm by sight. *Science*, 290(5497):1782–1786.

Graziano, M. S., Taylor, C. S., and Moore, T. (2002). Complex movements evoked by microstimulation of precentral cortex. *Neuron*, 34(5):841–851.

Head, H. and Holmes, G. (1911). Sensory disturbances from cerebral lesions. *Brain*, 34(2-3):102–254.

Hoffmann, M., Marques, H. G., Hernandez Arieta, A., Sumioka, H., Lungarella, M., and Pfeifer, R. (2010). Body schema in robotics: a review. *Autonomous Mental Development, IEEE Transactions on*, 2(4):304–324.

Iriki, A., Tanaka, M., and Iwamura, Y. (1996). Coding of modified body schema during tool use by macaque postcentral neurones. *Neuroreport*, 7(14):2325–2330.

Kohonen, T. (1982). Self-organized formation of topologically correct feature maps. *Biological cybernetics*, 43(1):59–69.

Lupashin, S., Schollig, A., Sherback, M., and D'Andrea, R. (2010). A simple learning strategy for high-speed quadrocopter multi-flips. In *Robotics and Automation (ICRA), 2010 IEEE International Conference on*, pages 1642–1648. IEEE.

Martinetz, T., Schulten, K., et al. (1991). *A" neural-gas" network learns topologies*. University of Illinois at Urbana-Champaign.

Melzack, R. (1990). Phantom limbs and the concept of a neuromatrix. *Trends in neurosciences*, 13(3):88–92.

Morasso, P. and Sanguineti, V. (1995). Self-organizing body schema for motor planning. *Journal of Motor Behavior*, 27(1):52–66.

Purwin, O. and D'Andrea, R. (2009). Performing aggressive maneuvers using iterative learning control. In *Robotics and Automation, 2009. ICRA'09. IEEE International Conference on*, pages 1731–1736. IEEE.

Ramachandran, V. S. and Rogers-Ramachandran, D. (1996). Synaesthesia in phantom limbs induced with mirrors. *Proceedings of the Royal Society of London. Series B: Biological Sciences*, 263(1369):377–386.

Sepulchre, R., Jankovic, M., and Kokotovic, P. (1997). *Constructive Nonlinear Control*. Springer-Verlag.

Stoytchev, A. (2003). Computational model for an extendable robot body schema.

Tsukamoto, Y. (2000). Pinpointing of an upper limb prosthesis. *JPO: Journal of Prosthetics and Orthotics*, 12(1):5–6.